Volume xx (200y), Number z, pp. 1-4

Approximating Planar Conformal Maps Using Regular Polygonal Meshes

Renjie Chen[1] and Craig Gotsman[2]

[1]Max Planck Institute for Informatics, Saarbrücken, Germany
[2]Jacobs Technion-Cornell Institute, Cornell Tech, New York, USA

Abstract

Continuous conformal maps are typically approximated numerically using a triangle mesh which discretizes the plane. Computing a conformal map subject to user-provided constraints then reduces to a sparse linear system, minimizing a quadratic "conformal energy". We address the more general case of non-triangular elements, and provide a complete analysis of the case where the plane is discretized using a mesh of regular polygons, e.g. equilateral triangles, squares and hexagons, whose interiors are mapped using barycentric coordinate functions. We demonstrate experimentally that faster convergence to continuous conformal maps may be obtained this way. We provide a formulation of the problem and its solution using complex number algebra, significantly simplifying the notation. We examine a number of common barycentric coordinate functions and demonstrate that superior approximation to harmonic coordinates of a polygon are achieved by the Moving Least Squares coordinates. We also provide a simple iterative algorithm to invert barycentric maps of regular polygon meshes, allowing to apply them in practical applications, e.g. for texture mapping.

Categories and Subject Descriptors (according to ACM CCS): I.3.8 [Computer Graphics]: Applications

1 Introduction

Conformal maps of planar domains are important in computer graphics and image processing, as they preserve the local proportions of the map, thus minimizing the inevitable visual distortion introduced by the mapping. Particularly popular in image and 3D model deformation applications, they are also used in animation scenarios. While conformal maps have been studied for decades in classical complex analysis, using them in real-world digital applications requires a discrete theory which has been developed only over the past decade. This typically involves discretizing the plane using a Finite-Element triangle mesh and computing a map, subject to user-supplied constraints, of this mesh into the deformed shape.

In this paper we depart from the typical triangle mesh scenario and address the more general case of higher-order polygons. We provide a complete analysis of the case where the plane is discretized using a mesh of regular polygons, e.g. equilateral triangles, squares and hexagons. We show that approximations that converge more rapidly to continuous conformal maps may be obtained this way.

Our approach is to analyze a broad family of *barycentric* maps between polygons based on so-called *barycentric coordinates* [Flo15]. We provide the basic theory required to compute these discrete maps and use them in practice.

2 Conformal and Harmonic Maps

We start by reviewing the necessary theory from complex and harmonic analysis. We provide only the very basics here and refer the reader to the classic book by Ahlfors [Ahl79] for a complete exposition of complex analysis. As we will see, it is particularly advantageous and compact to work with complex number algebra, despite the fact that in the end barycentric coordinates are real and everything could be described in $\mathbb{R}^2$. Identifying the 2D plane with the complex field $\mathbb{C}$, any complex-valued function from $\mathbb{C}$ to itself may be expressed as two real functions of the complex variable $z = x + iy$ and its conjugate $\bar{z} = x - iy$:

$$f(z, \bar{z}) = f_x(z, \bar{z}) + i f_y(z, \bar{z})$$

implying the complex *Wirtinger derivatives* [Ahl79]:

$$\frac{\partial}{\partial z} = \frac{1}{2}\left(\frac{\partial}{\partial x} - i\frac{\partial}{\partial y}\right), \quad \frac{\partial}{\partial \bar{z}} = \frac{1}{2}\left(\frac{\partial}{\partial x} + i\frac{\partial}{\partial y}\right)$$

2.1 Conformal maps

A complex-valued function f is *holomorphic* (also called *analytic*) iff it satisfies the Cauchy-Riemann equations:

$$\frac{\partial f_x}{\partial x} = \frac{\partial f_y}{\partial y}, \quad \frac{\partial f_x}{\partial y} = -\frac{\partial f_y}{\partial x}$$

or, more compactly,

$$i\frac{\partial f}{\partial x} = \frac{\partial f}{\partial y}$$

Alternatively, using the Wirtinger derivatives yields the very natural equivalent:

$$\frac{\partial f}{\partial \bar{z}} = 0 \tag{1}$$

Now, recall that a conformal map is actually a holomorphic function whose derivative $\frac{\partial f}{dz}$ is everywhere non-zero. Ignoring the non-zero derivative requirement for the moment, (1) leads to an natural measure of how non-conformal a map f is at a point z: $\left|\frac{\partial f}{d\bar{z}}\right|^2$. Thus the *conformal energy* of a mapping f of a domain $P \subset \mathbb{C}$ is defined as:

$$C(f) = 2\iint_P \left|\frac{\partial f}{\partial \bar{z}}\right|^2 dz \wedge d\bar{z} \tag{2}$$

(the $dz \wedge d\bar{z}$ indicates a two-dimensional area integral over P) and a mapping f is conformal on P iff $\frac{\partial f}{dz} \neq 0$ on P and $C(f) = 0$. The factor 2 in the definition of $C(f)$ is required for consistency with other definitions, as will be made clear later. For example, since an affine map may be expressed in general as $f(z) = az + b\bar{z} + c$, its conformal energy over a domain P is $C(f) = 2Area(P)|b|^2$ and an affine map is conformal iff it is *linear* in z: $f(z) = az + c$, which means that the map is just a similarity of the plane (i.e. a combination of translation, rotation and scaling).

Analogously to (1), an *anti-holomorphic* function f is one such that

$$\frac{\partial f}{\partial z} = 0$$

The simplest such function is $f(z) = \bar{z}$, which is just a reflection of the plane (through the x axis).

2.2 Harmonic maps

It is useful to relate the conformal energy (2) of a complex-valued map to the well-known classical concept of *Dirichlet* energy [PP93] of a real function. For a real function of two variables $f(x, y)$: $\mathbb{R}^2 \to \mathbb{R}$, the Dirichlet energy is defined on the domain $P \subset \mathbb{R}^2$ as:

$$D(f) = \frac{1}{2}\iint_P \left(\left|\frac{\partial f}{\partial x}\right|^2 + \left|\frac{\partial f}{\partial y}\right|^2\right) dxdy \tag{3}$$

and noting that, by definition,

$$\frac{\overline{\partial f}}{\partial z} = \frac{\partial \bar{f}}{\partial \bar{z}} \text{ and } \left|\frac{\partial f}{dz}\right|^2 = \frac{\partial f}{dz}\frac{\overline{\partial f}}{dz} = \frac{\partial f}{dz}\frac{\partial \bar{f}}{\partial \bar{z}}$$

we obtain

$$\left|\frac{\partial f}{\partial x}\right|^2 + \left|\frac{\partial f}{\partial y}\right|^2 = \left|\frac{\partial f}{\partial \bar{z}} + \frac{\partial f}{\partial z}\right|^2 + \left|\frac{1}{i}\left(\frac{\partial f}{\partial \bar{z}} - \frac{\partial f}{\partial z}\right)\right|^2 = 2\left(\left|\frac{\partial f}{\partial z}\right|^2 + \left|\frac{\partial f}{\partial \bar{z}}\right|^2\right)$$

Thus, (3) is equivalent to:

$$D(f) = \iint_P \left(\left|\frac{\partial f}{\partial z}\right|^2 + \left|\frac{\partial f}{\partial \bar{z}}\right|^2\right) dz \wedge d\bar{z} \tag{4}$$

which allows us to generalize the concept of Dirichlet energy to complex-valued functions.

Harmonic maps have been extensively studied (see, e.g. [Dur04]). The standard definition is by minimization of the Dirichlet energy:

A map f of a domain P to a domain Q is *harmonic* iff

$$f = \arg\min D(f) \quad s.t.\ f(\partial P) = f_{bound} \tag{5}$$

which can be shown to be equivalent to satisfaction of the Laplace equation, subject to given boundary conditions f_{bound}:

$$\nabla^2 f = \frac{\partial^2 f}{\partial z \partial \bar{z}} = 0 \quad s.t.\ f(\partial P) = f_{bound}$$

Harmonic and holomorphic functions are intimately related, as follows:

- The real and imaginary parts of a holomorphic function are harmonic. These functions are called *harmonic conjugates*.
- A function is harmonic iff it is the sum of a holomorphic function and an anti-holomorphic function.

A simple example of a harmonic map is the affine map $f(z) = az + b\bar{z} + c$, which, as mentioned above, is also holomorphic iff $b = 0$.

It is also easy to express the Jacobian determinant of a mapping using the Wirtinger derivatives:

$$J(f) = \frac{\partial f_x}{\partial x}\frac{\partial f_y}{\partial y} - \frac{\partial f_x}{\partial y}\frac{\partial f_y}{\partial x} = \left|\frac{\partial f}{\partial z}\right|^2 - \left|\frac{\partial f}{\partial \bar{z}}\right|^2$$

So for any $f: P \to Q$

$$D(f) = \iint_P \left(\left|\frac{\partial f}{\partial z}\right|^2 + \left|\frac{\partial f}{\partial \bar{z}}\right|^2\right) dz \wedge d\bar{z} = \iint_P \left(\left|\frac{\partial f}{\partial z}\right|^2 - \left|\frac{\partial f}{\partial \bar{z}}\right|^2\right) dz \wedge d\bar{z} + 2\iint_P \left|\frac{\partial f}{\partial \bar{z}}\right|^2 dz \wedge d\bar{z} = A_Q + C(f)$$

where A_Q is the signed area of Q. Consequently, in applications where P and Q are given, and the objective is to design a mapping between them (e.g. the polygon mapping problem described in the next subsection), the fact that A_Q is constant implies that the Dirichlet and conformal energies are minimized together.

2.3 Polygon mapping vs. point mapping

We now examine the following two mapping problems: the so-called *polygon mapping* problem and the *point mapping* problem (see Fig. 1). In the polygon mapping problem, two polygons $P = (p_1, .., p_n)$ and $Q = (q_1, .., q_n)$ with the same number of vertices are given, with a mapping between the boundaries of P and Q such that the edges are mapped linearly to each other, namely,

$$f(tp_{j+1} + (1-t)p_j) = tf(p_{j+1}) + (1-t)f(p_j) = tq_{j+1} + (1-t)q_j$$

The problem is then to compute the mapping between P and Q which satisfies these boundary conditions and is the most conformal, i.e.

$$f = \arg\min C(f) \tag{6}$$
$$s.t.\ f(tp_{j+1} + (1-t)p_j) = tq_{j+1} + (1-t)q_j \ \ \forall t \in [0,1]$$

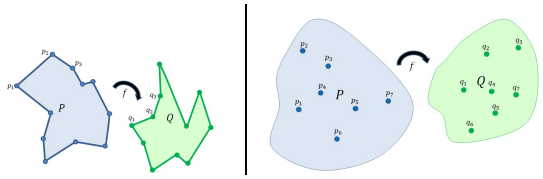

Figure 1: *Two possible mapping scenarios: **(left)** polygon mapping **(right)** point mapping.*

In the point mapping problem, the constraints are not given via boundary values, but by the images $q_i \in \mathbb{C}$ of a finite set of points $p_j \in P$. Thus we seek a continuous complex function $f: P \to \mathbb{C}$:

$$f = \arg\min C(f) \quad s.t. \quad f(p_j) = q_j \tag{7}$$

For the polygon mapping problem, there always exists a (unique) harmonic map satisfying the given boundary conditions. This is the classical *Dirichlet problem* (5) [Ahl79, Dur11]. In contrast, a conformal map satisfying those boundary conditions typically does *not* exist. It is overdetermined, as the celebrated Riemann mapping theorem [Ahl79] states that there is essentially just *one* conformal mapping of P to Q mapping ∂P to ∂Q (up to a very small number of degrees of freedom). Thus the best that can be hoped for is a map which minimizes the conformal energy subject to the boundary conditions, as in (6). Following the discussion at the end of Section 2.2, this is exactly the harmonic map of (5).

For the point mapping problem, since complete boundary conditions are not prescribed, many harmonic maps could satisfy the point constraints, and more information is needed to uniquely specify it. However, the constraints will typically overdetermine a conformal map, so here again, the conformal energy should be minimized, as in (7). Note, however, that the resulting map is *not* neccesarily harmonic.

In the sequel, we will combine the two (polygon mapping and point mapping) problems. The end-user problem will be a point mapping problem, which is useful in interactive deformation scenarios. This is solved using a FEM discretization of the plane, where our finite elements will be regular polygons, each mapped to its image as in the polygon mapping problem. We will sometimes call this discrete approximation of the continuous conformal map a *discrete conformal map.*

3 The Conformal/Dirichlet Energy of a Single Polygon

Assume the polygon mapping scenario, namely that the interior of a polygon P having n vertices is mapped to the interior of another polygon Q having the same number of vertices, in such a way that $f(p_j) = q_j$ and the edges are mapped linearly to each other. We now wish to compute the conformal energy of this mapping, which is the Dirichlet energy up to the area of Q. To do this, we need to specify the mapping, and we will restrict our attention to a well-known family of mappings – the *barycentric* mappings – which all satisfy the linear edge-to-edge boundary conditions. We begin with the general theory, and then specialize to the case where P is a regular polygon. We start first with the mapping of the simplest possible polygon - the triangle.

3.1 The triangle

Assume a triangle whose (column) vertex vector $z = (z_1, z_2, z_3)^t$ is affinely mapped to a triangle with vertex vector $w = (w_1, w_2, w_3)^t$. This mapping, of course, satisfies the linear edge-to-edge boundary constraints and is also harmonic, so minimizes the Dirichlet energy among all possible mappings, and we aim to compute its conformal energy. The (complex) coefficients a, b, c of the affine map $f(z) = az + b\bar{z} + c$ thus satisfy the linear equations

$$\begin{pmatrix} z_1 & \bar{z_1} & 1 \\ z_2 & \bar{z_2} & 1 \\ z_3 & \bar{z_3} & 1 \end{pmatrix} \begin{pmatrix} a \\ b \\ c \end{pmatrix} = \begin{pmatrix} w_1 \\ w_2 \\ w_3 \end{pmatrix}$$

Denoting the edge vectors $e_1 = z_2 - z_3$, $e_2 = z_3 - z_1$, $e_3 = z_1 - z_2$, $e = (e_1, e_2, e_3)^t$, the solution is $a = \frac{i}{4A_z} e^* w$, $b = -\frac{i}{4A_z} \bar{e}^* w$, where $A_z = \frac{1}{4i}(z_1\bar{e_1} + z_2\bar{e_2} + z_3\bar{e_3})$ is the area of the triangle with vertex vector z and $*$ is the conjugate transpose operator. Thus the conformal energy of the mapping may be expressed as a Hermitian form in w:

$$C(w) = 2A_z|b|^2 = 2A_z b^* b = w^* C w \tag{8}$$

where C is the scaled 3x3 outer product matrix $C = \frac{1}{8A_z} \overline{ee^*}$. The (j,k) entry of C can be seen to be $\frac{1}{4}(i + \cot\alpha_{jk})$, where α_{jk} is the angle opposite the edge between vertices j and k. See Fig. 2. This is consistent with the way the celebrated triangle mesh Laplacian (also known as cotangent weights) is constructed [DMA02, LM02, PP93].

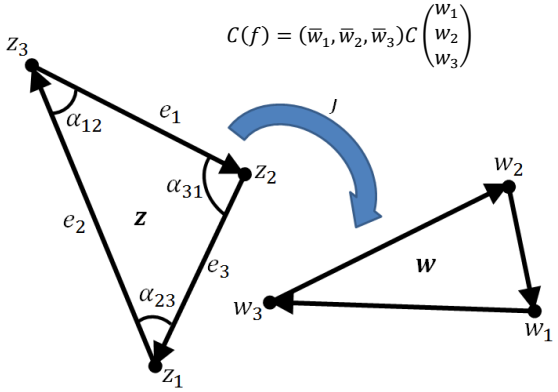

Figure 2: *An affine map f of the triangle z to the triangle w. The conformal energy $C(f)$ of this mapping is a Hermitian form on the vector $(w_1, w_2, w_3)^t$ with a 3x3 matrix C derived from the geometry of the triangle z.*

Note that, by definition, C has rank 1, and its nullspace is easily seen to be spanned by the two vectors $o = (1,1,1)^t$ and $z = (z_1, z_2, z_3)^t$. This is consistent with the fact that any triangle with vertex vector w which is a complex-valued linear function (a similarity) of the vertex vector z, i.e. $w = az + c$ will have vanishing conformal energy $C(w)$.

3.2 Higher-order polygons

We now show how to generalize the quadratic conformal energy (8) developed in the previous section to polygons with more than three sides. For this to be meaningful, we must specify how the interior of the source polygon P with vertices $z_1, .., z_n$ is mapped to the interior of the target polygon

Q with vertices $w_1,..,w_n$. We focus our attention on the so-called *barycentric* mappings, where a basis function $B_j(z)$ is associated with the j'th source polygon vertex. The basis functions have the following properties:

1. **Constant precision**: $\sum_{j=1}^{n} B_j(z) = 1,\ \forall z \in P$
2. **Linear precision**: $\sum_{j=1}^{n} z_j B_j(z) = z,\ \forall z \in P$
3. **Lagrange property**: $B_j(z_k) = \delta_{jk}$

Note that although we write $B_j(z)$, seemingly implying that B_j is a function of only z, B_j is usually non-holomorphic, i.e. a function of both z and $\bar{z}$, although we will omit the $\bar{z}$ argument for brevity's sake. Properties 1-3 imply that each source polygon edge is mapped linearly to its target counterpart. We may then define the function f on P as follows:

$$f(z) = \sum_{j=1}^{n} B_j(z) w_j$$

Over the years, many recipes for $B_j(z)$have been proposed, the most well-known being the so-called *three-point* schemes [FHK06]: Laplace [DMA02, LM02, PP93] (also called *discrete harmonic* or *cotangent*), mean value [Flo03, HF06], Wachspress [Wac75], and the harmonic scheme [JMD*07]. The first four have closed-form expressions, while the harmonic coordinates must be computed numerically by solving a Laplace equation with appropriate Dirichlet boundary conditions on P.

Weber et al. [WBGH11] expressed the three-point barycentric coordinate functions as follows:

$$\hat{B}_j(z) = \gamma_j(z)\frac{r_{j+1}(z)}{e_j} - \gamma_{j-1}(z)\frac{r_{j-1}(z)}{e_{j-1}},\ \ B_j(z) = \frac{\hat{B}_j(z)}{\sum_{j=1}^{n}\hat{B}_j(z)} \quad (9)$$

where $z_j, j = 1,..,n$ are the source polygon vertices, z is a point in the source polygon interior $r_j(z)$ is the difference $z_j - z$, e_j is the edge vector $z_{j+1} - z_j$ and γ_j is a complex function associated with the j'th edge. See Fig. 3. They show that the Wachspress, mean-value and Laplace coordinates may be obtained for

$$\gamma_j(z) = \frac{e_j}{\mathrm{Im}(\overline{r_j(z)} r_{j+1}(z))}\left(\frac{|r_{j+1}(z)|^p}{r_{j+1}(z)} - \frac{|r_j(z)|^p}{r_j(z)}\right) \quad (10)$$

with $p = 0, 1, 2$, respectively.

Not surprisingly, for the case of a triangle, all these coordinate functions are equivalent and reduce to the classical unique barycentric coordinates introduced by Moebius:

$$\hat{B}_j(z) = \frac{\mathrm{Im}(\bar{r}_{j-1}(z) r_{j+1}(z))}{\mathrm{Im}(\bar{e}_{j-1}(z) e_{j+1}(z))}$$

i.e. the ratio between the area of the triangle (z_{j-1}, z, z_{j+1}) with cyclic indexing to the area of the triangle (z_1, z_2, z_3). These coordinates induce the obvious affine mapping between the two triangles.

For a higher-order polygon with n sides, different choices of barycentric coordinate functions induce different mappings. In these cases, the conformal energy may be computed as follows:

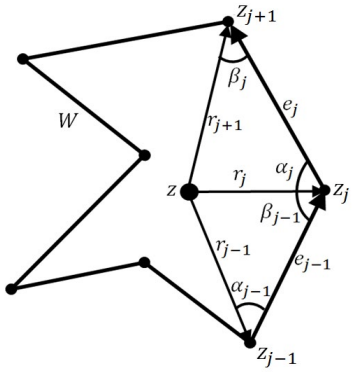

Figure 3: *The terminology of complex barycentric coordinates.*

$$\begin{aligned} C(f) &= 2\iint_P \left|\frac{\partial f}{d\bar{z}}\right|^2 dz \wedge d\bar{z} \\ &= 2\iint_P \left|\sum_{j=1}^{n} \frac{\partial B_j(z)}{\partial \bar{z}} w_j\right|^2 dz \wedge d\bar{z} \\ &= w^* C w \end{aligned} \quad (11)$$

where C is the $n \times n$ Hermitian *conformal matrix*

$$C_{jk} = 2\iint_P \frac{\partial B_j(z)}{\partial \bar{z}} \frac{\partial \bar{B}_k(z)}{\partial z} dz \wedge d\bar{z} \quad (12)$$

If P is a convex polygon the integrals (11) and (12) will typically exist. This is not the case for a non-convex P, since some of the barycentric coordinate functions may not be smooth or even continuous. If these integrals do exist, C has properties similar to the triangle case, as the following theorem shows:

Theorem 1: The conformal matrix C of an n-gon is positive semi-definite and has co-rank 2. Its nullspace is spanned by the all-ones vector $o = (1,..,1)^t$ and the source polygon geometry vector $z = (z_1,..,z_n)^t$.

Proof. C is positive semi-definite because it is a covariance matrix. Denote by $\{\psi_j : j = 1,..,n\}$ the (unit-length) eigenvectors of C. Consider the barycentric mapping B_j of the (source) polygon to a target polygon whose vertices are the entries of ψ_j with linear (edge-to-edge) boundary conditions. By definition, the eigenvalue λ_j associated with ψ_j is the conformal energy, implying that $\lambda_j = 0$ iff the mapping B_j is conformal. Now the constant mapping $B_1(z) \equiv 1$ and the identity mapping $B_2(z) = z$ are certainly conformal and satisfy the linear boundary conditions, thus the two independent vectors o and z are contained in $null(C)$ (as are all vectors $az + bo$ for any complex scalars a and b, which represent an arbitrary similarity of the plane). Any other eigenvector ψ_j not spanned by o and z represents a target polygon which is not a similar copy of z, thus the mapping B_j will be piecewise linear on the boundaries with a derivative discontinuity at one vertex at least. This implies that B_j is not differentiable at that vertex, thus cannot be conformal. As a result, its conformal energy is positive, namely $\lambda_j > 0$. ■

As we will see, the matrix C will play a central role in the sequel. A similar *stiffness matrix* is used in Finite Element Methods (FEM), as described by Sukumar and Malsch

[SM06], and the subsequent development of the so-called Virtual-Element Method (VEM) [MRS14]. These investigated the solution of second-order elliptic differential equations, in particular the Poisson equation, using FEM with mesh elements which are general polygons. Since all the mesh elements are typically different from each other, the method requires the computation of the (different) stiffness matrix of each element, a significant computational task in itself. Thus the focus of Sukumar and Malsch's work [SM06] is the accurate computation of the stiffness matrix of an arbitrary polygon and determining which barycentric coordinate (basis) functions yield the most accurate solution to the Poisson equation. They conclude that for convex elements, the Laplace elements achieve the best approximation. Although playing a similar role, our matrix C, being *complex-valued* and more compact, differs from the classical *real-valued* stiffness matrix. Furthermore, in the sequel we will focus on *regular* polygonal elements, which have special properties and can be analyzed in more detail. Conveniently, using a mesh of identical regular elements avoids the need to compute a separate matrix per mesh element.

3.3 Circular polygons

There are a number of special cases which result in interesting conformal energy matrices. Consider a *circular* polygon P, namely a polygon whose vertices all lie on a circle S, (sometimes called a *cyclic* polygon) and consider the piecewise-affine mapping induced by some triangulation of P. In this case all possible triangulations of P are Delaunay (since, by definition, the circumcircles of all possible triangles lie on S), thus all entries of C corresponding to interior edges of P will have vanishing entries (since the two angles α and β opposite the edge sum to π, implying $\cot\alpha + \cot\beta = 0.$)

Another interesting property of circular polygons, shown by Floater et al [Flo15], is that the Laplace and Wachspress barycentric coordinates are identical for these polygons.

4 Regular Polygons

The most interesting special case – the one we will concentrate on from now on – is that of a regular polygon, in particular the equilateral triangle, the square and the regular hexagon, which may be used to tile the plane. The symmetry of the polygon dictates that barycentric coordinate functions will be identical up to rotation of the variable z. Without loss of generality, assume that the polygon P's vertices z_j are the n'th roots of unity:

$$\omega_n = \exp\left(\frac{2\pi i}{n}\right), \qquad z_j = \omega_n^{j-1}, \quad j = 1,..,n$$

Since a regular polygon is circular, the properties mentioned in the previous section carry over to this case.

Because of the rotational symmetry, the $n \times n$ conformal energy matrix C will be circulant, spanned by the row

$$C_{1k} = 2\iint_P \frac{\partial B_1(z)}{\partial \bar{z}} \frac{\partial \bar{B}_k(z)}{\partial z}\, dz \wedge d\bar{z}$$

and have the Fourier vectors as its eigenbasis:

$$\varphi_{kj} = \omega_n^{(j-1)(k-1)}$$

So its first eigenvector ($k = 1$) will be the all-ones vector $o = (1,..,1)^t$, and the second eigenvector ($k = 2$) will be the polygon geometry vector z. By Theorem 1, these two eigenvectors will have vanishing eigenvalues, and all other eigenvectors will have positive eigenvalues. Thus, for any barycentric coordinate recipe, the matrix C may be written as the sum of $n-2$ outer products of the Fourier eigenvectors, weighted by their corresponding eigenvalues:

$$C = \sum_{k=3}^{n} \lambda_k (\varphi_k \varphi_k^*) \tag{13}$$

meaning that the specific barycentric coordinate scheme used is characterized by the conformal matrix spectrum of $n-2$ positive values $\lambda_k, k = 3,..,n$. Note that since an arbitrary scaling of C by a positive real constant will essentially not change the energy function, there are actually only $n-3$ degrees of freedom in C, and even then, not all possible values of λ_k are allowed, namely, correspond to some barycentric coordinate recipe.

The following theorem shows that the conformal matrix spectra of *any* real barycentric coordinate functions on a regular polygon actually have another eigenvalue in common, apart from the two zeros:

Theorem 2: The spectrum of the conformal matrix of *any* real barycentric coordinate functions on a regular n-gon contains $\lambda_n = \sin\frac{2\pi}{n}$.

Proof: As for *any* circulant matrix, the eigenvectors of the circulant conformal matrix of all barycentric coordinate functions on a n-sided regular polygon $P_n = (z_1, z_2, .., z_n)$ $= (\omega_n^0, \omega_n^1 .., \omega_n^{n-1})$ are the Fourier vectors:

$$\varphi_j = \left(\omega_n^0, \omega_n^{j-1}, .., \omega_n^{(n-1)(j-1)}\right)^t \qquad j = 1,..,n$$

with eigenvalues $\lambda_1, .., \lambda_n$. Denote by $B_j(z), j = 1,.,n$ the n barycentric coordinate functions, and by C the associated conformal energy matrix of P.

Now we observe that, since any unit-length complex number u satisfies $u^{-1} = \bar{u}$,

$$\begin{aligned}\varphi_n &= \left(\omega_n^0, \omega_n^{n-1}, .., \omega_n^{(n-1)(n-1)}\right)^t \\ &= \left(\omega_n^0, \omega_n^{-1}, .., \omega_n^{-1(n-1)}\right)^t \\ &= (\omega_n^0, \bar{\omega}_n, .., \bar{\omega}_n^{n-1})^t = \overline{\varphi_2}\end{aligned}$$

So, since $B_i(z)$ are real, for the target polygon φ_n

$$f(z) = \sum_{j=1}^{n} B_j(z)\, \varphi_n = \sum_{j=1}^{n} \bar{B}_j(z)\, \bar{\varphi}_2 = \overline{\sum_{j=1}^{n} B_j(z)\, \varphi_2} = \bar{z}$$

The conformal energy of this mapping $f(z) = \bar{z}$ is

$$\begin{aligned}E_c(f) &= 2\iint_P \left|\frac{\partial f}{d\bar{z}}\right|^2 dz \wedge d\bar{z} = 2\iint_P dz \wedge d\bar{z} \\ &= 2\text{Area}(P) = n\sin\frac{2\pi}{n}\end{aligned}$$

Since the conformal energy is also $E_C(f) = \varphi_n^* C \varphi_n = \lambda_n |\varphi_n|^2 = n\lambda_n$, we conclude that $\lambda_n = \sin\frac{2\pi}{n}$. ■

Corollary 1: For $n = 3, 4, 6$, we have $\lambda_n = \frac{\sqrt{3}}{2}, 1, \frac{\sqrt{3}}{2}$ respectively. ■

We now study the important special cases of regular polygons for $n = 3, 4, 6$ when mapped using the following barycentric coordinates: Triangulated (T), Wachspress (W) [Wac75] = Laplace (L) [PP93], mean value (MV) [Flo03], affine-based Moving Least Squares (MLS) [MS10], Gordon-Wixom (GW) [GW74], Improved Gordon-Wixom (IGW) [BF15] and harmonic (H) [JMD*07]. Each will have a different conformal energy matrix, but with common (Fourier) eigenstructure. Since the conformal energy is minimized for the harmonic mapping (H), we expect this to reflect in the spectrum of its conformal matrix.

4.1 The equilateral triangle

The simplest regular polygon is the equilateral triangle, with vertices vector $z = \left(1, -\frac{1-\sqrt{3}i}{2}, -\frac{1+\sqrt{3}i}{2}\right)^t$. The barycentric coordinates are uniquely determined by the affine mapping:

$$B_k(z) = \frac{1}{3}\mathrm{Re}\left(1 + 2z\omega_3^{1-k}\right), \qquad k = 1,2,3$$

Accordingly, there is just one possible conformal matrix, as developed in Section 3.1.

$$C = \frac{1}{24\sqrt{3}}\overline{\begin{pmatrix} -3-\sqrt{3}\imath \\ 3-\sqrt{3}\imath \\ 2\sqrt{3}\imath \end{pmatrix}\begin{pmatrix} -3-\sqrt{3}\imath \\ 3-\sqrt{3}\imath \\ 2\sqrt{3}\imath \end{pmatrix}^*} = \frac{1}{4\sqrt{3}}\begin{pmatrix} 2 & -1+\sqrt{3}i & -1-\sqrt{3}i \\ -1-\sqrt{3}i & 2 & -1+\sqrt{3}i \\ -1+\sqrt{3}i & -1-\sqrt{3}i & 2 \end{pmatrix}$$

with spectrum $\left(0,0,\frac{\sqrt{3}}{2}\right)$.

4.2 The square

The regular polygon with $n = 4$ sides is the square with vertices vector $z = (1, i, -1, -i)^t$. For this polygon the Wachspress and Laplace barycentric mappings are identical, as for all circular polygons, but for the square these are also identical to the bilinear and harmonic coordinates:

$$B_k(z) = \frac{1}{4}\mathrm{Re}\left(\left(1 + z\omega_4^{1-k}\right)^2\right), \qquad k = 1 \ldots 4 \qquad (14)$$

Table 1 shows the two non-zero eigenvalues of the conformal energy matrix corresponding to the different barycentric mappings of the square, along with the first row of the circulant matrix itself. These integrals were computed symbolically where possible, otherwise numerically by MATLAB's `integral2` function based on a quadrature on the square. MATLAB guarantees that the relative error in the computation is less than 10^{-6}. As expected, the harmonic (H) mapping has the smallest eigenvalues, consistent with the fact that it achieves the smallest conformal energy. The MLS coordinates are very close to these, indicating that they provide a superior approximation to harmonic coordinates.

Table 1
Conformal energy matrices and spectra of some barycentric mappings of the unit square

Barycentric coordinate	Conformal eigenvalues λ_4, λ_3	First row of conformal matrix
W = H = L = bilinear	$1, 1/3$	$\frac{1}{4}(4/3, -1/3 + i, -2/3, -1/3 - i)$
T	$1, 1$	$\frac{1}{4}(2, -1 + i, 0, -1 - i)$
MV	$1, .342065$	$\frac{1}{4}(1.342065, -0.342065 + i, -0.657935, -0.342065 - i)$
MLS	$1, .333635$	$\frac{1}{4}(1.333635, -0.333635 + i, -0.666365, -0.333635 - i)$
GW	$1, .350756$	$\frac{1}{4}(1.350756, -0.350756 + i, -0.649244, -0.350756 - i)$
IGW	$1, .355479$	$\frac{1}{4}(1.355479, -0.355479 + i, -0.644521, -0.355479 - i)$

4.3 The regular hexagon

The regular polygon with $n = 6$ sides is the hexagon with vertex vector $z = \left(1, \frac{1}{2} + \frac{\sqrt{3}}{2}, -\frac{1}{2} + \frac{\sqrt{3}}{2}, -1, -\frac{1}{2} - \frac{\sqrt{3}}{2}, \frac{1}{2} - \frac{\sqrt{3}}{2}\right)^t$. As in the cases $n = 3, 4$, here too the Wachspress (W) and Laplace (L) barycentric mappings are identical, but these do not coincide with the harmonic (H) coordinates, for which a closed-form expression does not exist.

Table 2 shows the four non-zero eigenvalues of the conformal energy matrix corresponding to some of the different barycentric mappings of the regular hexagon. In the non-harmonic case, the matrix was computed using a quadrature on a simple triangulation of the hexagon to four triangles (the quadrature on a triangle was obtained by duplicating and reflecting the triangle to form a parallelogram and then affinely transform it to a rectangle, which MATLAB's `integral2` function can handle). Here again, MATLAB guarantees error less than 10^{-6}. In the harmonic case, the matrix was computed over a dense triangulation of the hexagon into 14,000 triangles. The harmonic function was then approximated as a piecewise-linear interpolant and the integral computed analytically over each triangle. As in the case of a square, the harmonic mapping (H) has the smallest eigenvalues, consistent with the fact that it achieves the smallest conformal energy. The closest to this again seems to be the MLS coordinates.

Table 2
Conformal energy matrix spectra of some barycentric mappings of the regular hexagon

Barycentric coordinate	Conformal eigenvalues $\lambda_6, \lambda_5, \lambda_4, \lambda_3$ First row of conformal matrix
H	$\sqrt{3}/2, .924824, .413950, .058799$ $\frac{1}{4}(1.50907, -0.31517 + i, -0.34058, -0.19757, -0.34058, -0.31517 - i)$
T	$\sqrt{3}/2, \sqrt{3}, \sqrt{3}, \sqrt{3}/2$ $\frac{1}{4}(2\sqrt{3}, -\sqrt{3} + i, 0, 0, -\sqrt{3} - i)$
W = L	$\sqrt{3}/2, .929965, .422050, .063940$ $\frac{1}{4}(1.52132, -0.32399 + i, -0.33861, -0.19611, -0.33861, -0.32399 - i)$
MV	$\sqrt{3}/2, .934926, .434346, .068901$ $\frac{1}{4}(1.53613, -0.33550 + i, -0.33372, -0.19770, -0.33372, -0.33550 - i)$
MLS	$\sqrt{3}/2, .925390, .414526, .059364$ $\frac{1}{4}(1.51020, -0.31593 + i, -0.34058, -0.19720, -0.34058, -0.31593 - i)$
GW	$\sqrt{3}/2, .935107, .432956, .069082$ $\frac{1}{4}(1.53545, -0.33469 + i, -0.33477, -0.19653, -0.33477, -0.33469 - i)$
IGW	$\sqrt{3}/2, .960167, .471829, .094142$ $\frac{1}{4}(1.59478, -0.37731 + i, -0.32556, -0.18903, -0.32556, -0.37731 - i)$

4.4 Some examples

To illustrate the difference between the different barycentric coordinate mappings, we show the deformations achieved when a single polygon is mapped by minimizing the conformal energy of the mapping subject to positional constraints on three of the vertices of the polygon, using the "triangle" (T) and harmonic (H) barycentric mappings. The image of the regular source polygon is an irregular polygon. The top row of Fig. 4 shows this for deformations of a square and Fig. 5 for deformations of a regular hexagon. The blue points show the positional constraints on the target polygon. As expected, there is a significant difference between the two. Not

shown are the deformations corresponding to the other barycentric coordinate scehemes, which are very similar to the harmonic result.

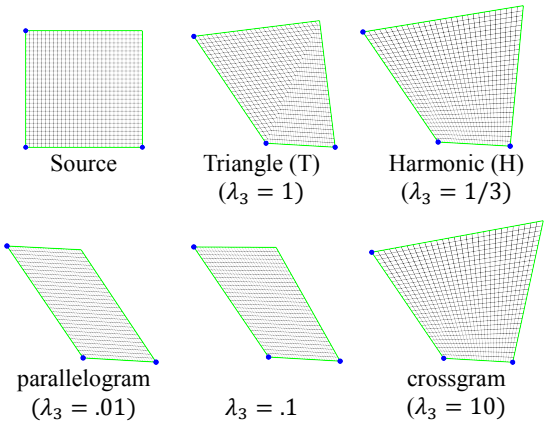

Figure 4: *Deformations of a square minimizing various energies. The first two (top row) are conformal energies associated with the two-triangle and harmonic barycentric mappings of the interior of the square. The grid texture allows to visualize the mapping. Note the discontinuity along the diagonal in the triangle (T) mapping. The next three (bottom row) are the result of minimizing an energy with $\lambda_4 = 1$ and values of λ_3 not corresponding to any barycentric mapping. Three of the vertices have been constrained. Note how very small values of λ_3 result in a parallelogram, and very large values in a "crossgram" – a quadrilateral in which the two diagonals have equal length and are perpendicular to each other.*

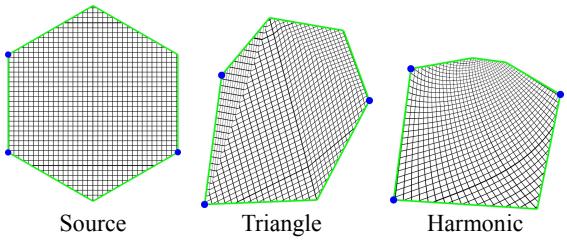

Figure 5: *Deformations of a regular hexagon minimizing conformal energy associated with different barycentric mappings of the interior. The grid texture allows to visualize the mapping.*

4.5 Non-barycentric energies

The conformal energy matrices described in Tables 1 and 2 above all correspond to barycentric mappings. However, it should be possible to use a matrix C as in (13) with arbitrary positive values of λ_k. This will probably not correspond to the conformal energy of any barycentric mapping, but perhaps result in other interesting effects. For example, take $\lambda_4 = 1$ and $\lambda_3 = \varepsilon$ (a very small number) in the square case $(n = 4)$ (we avoid taking $\lambda_3 = 0$ since then C would have rank 1). Minimizing this "energy" results in the square striving to be deformed to a parallelogram. Taking the opposite $\lambda_4 = 1$ and λ_3 to be a very large number results in the square deforming to a "crossgram" – a quadrilateral in which the two diagonals have equal length and are perpendicular to each other. This is demonstrated in the bottom row of Fig. 4 and has been explored in a recent paper of Chen and Gotsman [CG16], who used it to generate piecewise-affine mappings, approximating projective homographies of the plane. Interestingly, despite the fact that it does not really correspond to any conformal energy, the crossgram case was recently proposed by Cartade [CMMS13] for conformal deformations of quad meshes. They show also how to generalize it to arbitrary meshes.

5 Polygonal Meshes

A deformation of a single polygon is of limited interest in real-world applications. It is more useful to tessellate a planar region P with a polygonal mesh, and then compute a deformation of this entire mesh structure given positional constraints on a small subset of the mesh vertices, which have been specified by the application.

One of the most popular (and simplest) methods to compute a discrete map of P which is as close to conformal as possible is to triangulate the interior of P and, subject to the positional constraints, solve for the images of the vertices of the triangulation of P. The objective is that each triangle of P is mapped to a triangle which is, as much as possible, a similar copy of itself. This is called the As-Similar-As-Possible (ASAP) mapping [DMA02, LM02] and can easily be shown to boil down to a linear system of equations equivalent to the discrete linear Laplace equation, with boundary conditions which are not necessarily Dirichlet conditions (i.e. on the domain boundary). Since the set of *source* triangles in P and their images define a piecewise-affine mapping of the interior of P to $\mathbb{C}$, any point $p \in P$ may then be mapped uniquely using the appropriate affine mapping.

Note that a conformal map is by definition locally injective. In constrast, a discrete conformal map, particularly one generated by the FEM method, may not be so. This manifests in elements whose images have flipped orientation. Methods have been developed to generate mappings which avoid this (e.g. [SKPS13, PL14]), but we do not deal with this issue in this paper.

We now consider what happens when P is decomposed into elements which are not necessarily triangles, rather regular polygons, e.g. squares or regular hexagons, which are the only possible tessellations of the plane using identical regular elements. Since the conformal energy is additive, the conformal energy of a deformed complete mesh consisting of many *regular* polygons is simply the sum of their individual conformal energies (11) (or (8)). For a mesh of m vertices, this results in a $m \times m$ Hermitian matrix C, (analogous to the so-called *global stiffness matrix* of FEM) where the conformal energy is a quadratic form on the mesh vertex positions (when represented as complex numbers). The structure of C is very similar to that of the Laplacian matrix of a mesh [PP93], which is quite sparse, an entry of the matrix being non-zero only if it corresponds to a pair of vertices which are vertices of a common polygon. Typically, there will be a non-zero entry for every such pair of vertices, as observed by Alexa and Wardetzky [AW11]. However, if the individual conformal matrix used per polygon corresponds to the piecewise-triangle mapping, the only non-zero entries will correspond to the *edges* of the mesh, i.e. the Laplacian will have

the sparsity structure of the mesh adjacency matrix. This is called a *perfect* Laplacian [HKA15].

Fig. 6 shows some deformations of a rectangular planar region using different discretizations with regular polygons and two different barycentric interior mappings of the polygons – the triangle (T) mapping and the harmonic (H) mapping. Since the complexity of the linear system to be solved depends on the number of vertices in the mesh, for a fair comparison we used meshes containing approximately the same number of vertices ($m = 18$ on the average in the figure) covering the deforming region. All the deformations are subject to an identical set of (blue) point constraints, and the resulting deformation is visualized by a checkerboard texture map. Each square of the checkerboard is 8×8 image pixels and the edge length of the triangle, quad and hex were 90, 80 and 73 pixels, respectively. Each visualization is accompanied by E_C – the total conformal energy of the deformation. The results show that the "most conformal" deformation, both quantitavely and qualitatively, is achieved by hex elements using harmonic coordinates. Similar results are obtained when using many of the other barycentric coordinates (in particular MLS and MV) instead of the harmonic coordinates. To measure the convergence of the mapping as the resolution of the mesh is increased, we performed identical experiments for mesh sizes increasing up to $m =$ 30,000 vertices. Fig. 7 shows the performance statistics when the resolution of the mesh is increased. The left graph reports the decrease in conformal energy when an interior harmonic mapping is used, in a log-log plot. The linear behavior indicates an inverse polynomial relationship. The right graph reports the increase in runtime, as measured when using MATLAB's LDL solver, which performs well on sparse linear systems. Surprisingly, the quad mesh solves a little faster than the others, despite the associated matrix not being the least sparse - 8 entries per row on the average for interior mesh vertices - as opposed to 12 and 6 in the hexagonal and triangular case, respectively.

5.1 Solving the optimization problem

In practice, the positions of the deformed mesh vertices are derived by solving the set of linear normal equations corresponding to optimizing the quadratic conformal energy (subject to the linear point constraints).When a small set of mesh points are constrained, there is a simple analytic solution, which we detail here for completeness' sake: Denote by C the conformal matrix of the mesh. Denote by A and B the indices of the constrained and free sets of mesh vertices respectively, and by w_A and w_B the vector of their deformed positions, respectively. Without loss of generality, order the mesh vertices such that all constrained vertices come before the free vertices, and partition C as follows:

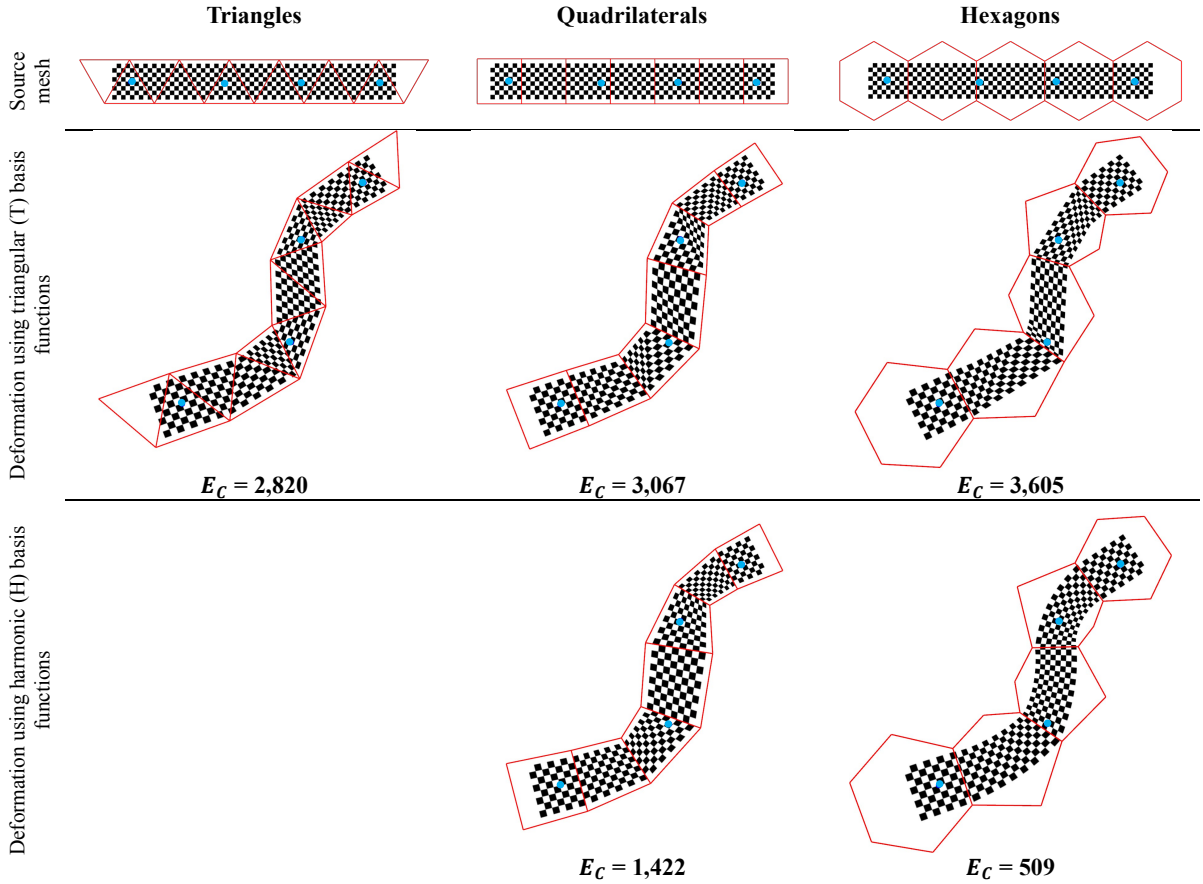

Figure 6: ***(Top)*** *Discretization of bar shape using regular triangles, quads and hexagonal elements. The edge lengths of the three types of elements are 90,80 and 73 image pixels, respectively. The bar is deformed using four (blue) constraints.* ***(Middle)*** *Deformation using conformal energy based on triangle (T) basis functions. (bottom) Deformation using conformal energy based on harmonic (H) basis functions. Note how smooth the harmonic deformation on hexagons is.*

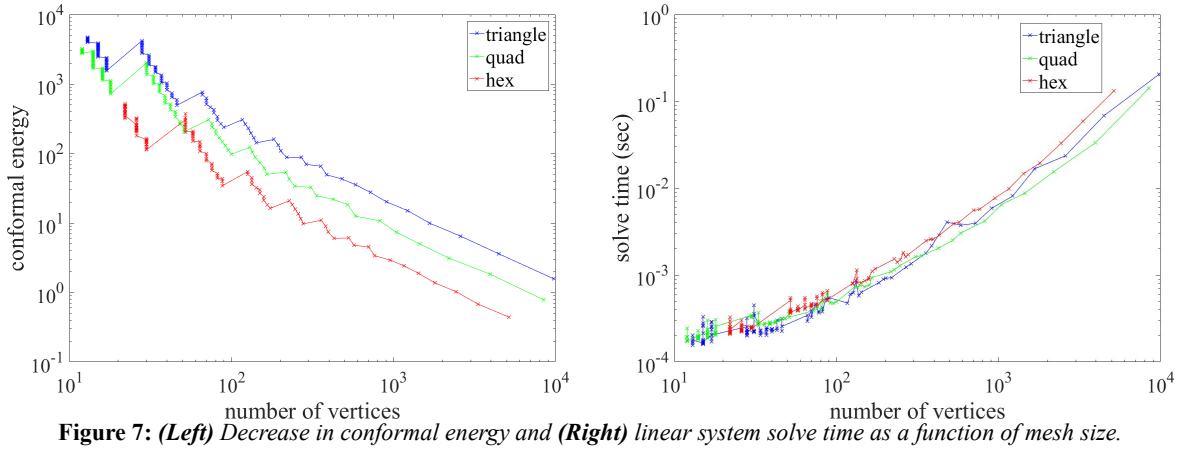

Figure 7: ***(Left)*** *Decrease in conformal energy and* ***(Right)*** *linear system solve time as a function of mesh size.*

$$C = \begin{pmatrix} C_{AA} & C_{AB} \\ C_{BA} & C_{BB} \end{pmatrix}$$

Then, given w_A, minimizing $C(w)$ implies the following set of normal equations for w_B:

$$(C_{BA} \quad C_{BB}) \begin{pmatrix} w_A \\ w_B \end{pmatrix} = 0$$

resulting in:

$$w_B = -C_{BB}^{-1} C_{BA} w_A \tag{15}$$

This can be interpreted as saying that the free vertex positions w_B are just a linear combination of the constrained vertex positions w_A, where the "basis functions" used in the linear combination depend only on the source mesh: the (j,k) entry of $-C_{BB}^{-1}C_{BA}$ represents the "influence" of the k'th constrained vertex on the j'th free vertex. Fig. 8 illustrates some of these basis functions on a regular hexagonal mesh. This is very similar to the concept of barycentric coordinates, except that here the constraints are points (as opposed to the edges of a polygon).

Using the same notation, the conformal energy of the deformed mesh may be rewritten as:

$$\begin{aligned} C(w) &= \begin{pmatrix} w_A \\ w_B \end{pmatrix}^* \begin{pmatrix} C_{AA} & C_{AB} \\ C_{BA} & C_{BB} \end{pmatrix} \begin{pmatrix} w_A \\ w_B \end{pmatrix} \\ &= \begin{pmatrix} w_A \\ w_B \end{pmatrix}^* \begin{pmatrix} C_{AA} w_A + C_{AB} w_B \\ 0 \end{pmatrix} \\ &= w_A^* C_{AA} w_A + w_A^* C_{AB} w_B \end{aligned}$$

Using (15):

$$\begin{aligned} &= w_A^* C_{AA} w_A - w_A^* C_{AB} C_{BB}^{-1} C_{BA} w_A \\ &= w_A^* (C_{AA} - C_{AB} C_{BB}^{-1} C_{BA}) w_A \end{aligned}$$

implying that the constrained conformal energy is still a quadratic form in the positions of just the constrained vertices w_A. Note that C_{AA} will typically be diagonal if the constrained vertices are distant from each other in the mesh. The observant reader will also note that the Hermitian matrix is the *Schur complement* [HJ13] of C.

In a practical deformation scenario, some of the user-supplied constraints will not coincide exactly with mesh vertices, but rather fall within a mesh polygon. In this case, the constraint location is expressed as a linear combination of the polygon vertices, again using barycentric coordinates. This still leads to a slightly more intricate linear system to solve for w_B.

5.2 Comparison to similarity-based mesh-free MLS mapping

It is interesting to compare the maps generated by minimizing conformal energy on discrete meshes to other ways of approximating continuous conformal maps. The Moving Least Squares (MLS) mappings, as introduced by Schaefer et al [SMW06], generates, given a set of point constraints, a continuous deformation which, per point z in the plane, computes the best similarity mapping S_z fitting the constraints, where each constraint z_k is weighted in some way depending on its proximity to z, e.g. by $|z - z_k|^{-2}$. The deformation is then defined to be $f(z) = S_z(z)$.

It is relatively straightforward to show that the MLS mapping can also be expressed as a linear combination of basis functions depending only on the positions of the constrained points in the *source*. Weighting the target positions of these constraints with the basis functions produces the final mapping. Fig. 8 depicts the basis functions of the mesh-free MLS method under the same conditions as a discrete conformal map based on a regular hex mesh, assuming each hex is mapped using a harmonic map. Note the local nature of the MLS basis functions, which, at first glance, would seem to be a desirable property. However, this also implies that the MLS mapping is unpredictable in regions distant from all the

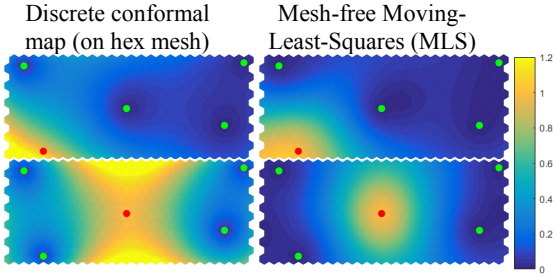

Figure 8: ***(left)*** *Two of the five basis functions of a discrete conformal map constrained at 5 points, computed on a hex mesh using the harmonic barycentric coordinate mapping per hex. Note how the basis functions increase in regions void of constraints.* ***(right)*** *Analogous two basis functions of the mesh-free MLS method. Note the locality of these basis functions.*

constraints. In contrast, the discrete conformal basis functions grow in regions void of constraints, keeping the mapping under control.

5.3 Weighted discrete conformal maps

As mentioned above, a conformal map of a polygonal mesh may be computed by minimizing the quadratic conformal energy of the mesh, where each polygon contributes proportionally to its area. This can easily be done differently if the application dictates that some region be mapped more conformally, possibly at the expense of other regions. All that needs to be done is to weight the contribution of each polygon by some positive real weight, depending on its importance. The resulting conformal energy matrix will still be Hermitian. A possible application is in image warping, where it is more important to conformally map the regions containing high frequencies, at the expense of regions which contain only low frequencies, under the premise that any distortion is less noticeable in those regions. This is sometimes called "content-aware" deformation and Fig. 9 shows a typical application: "image retargeting" [RGSS10]. Here the objective is to modify the aspect ratio of a given image, in this case transforming a rectangle into a square. This is implied by appropriate constraints along the entire boundary of the mesh, and would ordinarily just stretch the source image vertically. This is indeed what happens when uniform importance is used. In contrast, when weighted by a user-specified *importance map*, concentrating on the more interesting parts of the image, the result is a deformation that is more conformal (thus less distorting) in the regions of high importance, at the expense of the conformality in the other regions. Weighting the various elements in a conformal mapping scenario was also done by Mullen et al. [MTAD08], albeit in a 3D mesh parameterization scenario, where the weighting factor was simply the inverse of the element area.

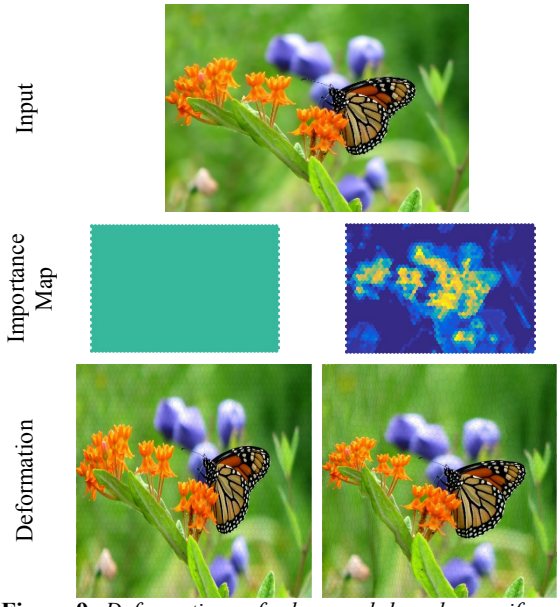

Figure 9: *Deformations of a hex mesh based on uniform and non-uniform importance maps. The constraints (along all the boundary vertices) imply a vertical stretch of the* ***(top)*** *input image, which is what is obtained with* ***(bottom left)*** *a uniform importance map. However, the non-uniform importance map causes* ***(bottom right)*** *some regions to be mapped more conformally than others, resulting in less distortion where it is visibly noticeable.*

6 Inverting Barycentric Maps

An important practical question arises when using barycentric mappings in a real-world application. In order to render a deformation of a given image, using, say, texture mapping, it is necessary to invert the mapping. For example, in order to render the image of the deformed grid in Fig. 9, it is necessary to invert all the barycentric mappings used on the interiors of the individual polygons.

This is, in general, a difficult problem. The simplest version of the problem – inverting the bilinear map of a unit square – has attracted some attention since bilinear maps of quads are quite popular in computer graphics. (Note that by bilinear we mean maps of the form (14), and not the conformal *linear fractional map*, which is sometimes also called a bilinear map). The exact solution involves solving a quadratic equation, i.e. computing a square root. While this does not sound difficult, it may suffer from numerical imprecision in single-precision shaders. In practice, the map is inverted using an iterative Gauss-Newton algorithm, which converges quite quickly. We now present an algorithm which works for all invertible barycentric mappings, working especially well if the mapping is close to conformal.

6.1 The "gamma" formulation of complex barycentric coordinates

Weber et al. [WBGH11] provided an alternative description of barycentric coordinates, when expressed using complex numbers. They show that, up to normalization, any barycentric coordinate function can be expressed as a linear combination (by so-called "gamma functions" $\gamma_j(z)$) of similarity transformations per edge, where the j'th similarity transformation S_j is derived from the j'th source-target edge pair, and then applied to a point z, weighted by $\gamma_j(z)$. This seems a more natural description in the context of conformal maps, since similarities are the simplest form of a conformal map.

More precisely, the γ formulation represents a barycentric mapping as

$$f(z) = \sum_{i=1}^{n} \gamma_j(z) S_j(z) \tag{16}$$

where the j'th similarity function is:

$$S_j(z) = f_j + a_j(z - z_j)$$

and the $a_j = \frac{\hat{e}_j}{e_j}$ are (complex-valued) constants depending only on the source and target polygons: $e_j = z_{j+1} - z_j$ and $\hat{e}_j = f_{j+1} - f_j$ are the j'th edge of the source and target polygons, respectively.

For example, the Laplace coordinate functions may be described using $\gamma_j(z) = \left|\frac{e_j}{h_j(z)}\right|$, where $|h_j(z)|$ is the distance of z from the j 'th edge, and normalizing so that $\sum_{i=1}^{n} \gamma_j(z) = 1$. Weber et al [WBGH11] provide a general

form of the γ functions for the family of three-point coordinates.

6.2 The iterative algorithm

We present here an iterative algorithm to invert a general barycentric mapping using its γ functions. Given $w = f(z)$, and assuming f is injective, we would like to compute z, i.e. solve the equation $w - f(z) = 0$ for z. The Newton-Raphson method over the complex field dictates the following iteration, given an initial guess z_0:

$$z_{n+1} = z_n + \frac{(w - f(z_n))\overline{\frac{\partial f}{\partial z}(z_n)} - \overline{(w - f(z_n))}\frac{\partial f}{\partial \bar{z}}(z_n)}{\left|\frac{\partial f}{\partial z}(z_n)\right|^2 - \left|\frac{\partial f}{\partial \bar{z}}(z_n)\right|^2} \qquad (17)$$

(note that the denominator in (17) is the Jacobian of f at z_n). Now, since $\sum_{i=1}^{n}\gamma_j(z) = 1$ implies $\sum_{i=1}^{n}\frac{\partial \gamma_j(z)}{\partial z} = 0$ and $\sum_{i=1}^{n}\frac{\partial \gamma_j(z)}{\partial \bar{z}} = 0$, from (16) we obtain:

$$\frac{\partial f}{\partial z} = \sum_{i=1}^{n}\frac{\hat{e}_j}{e_j}\gamma_j + \sum_{i=1}^{n} S_j \frac{\partial \gamma_j}{\partial z}$$

and

$$\frac{\partial f}{\partial \bar{z}} = \sum_{i=1}^{n} S_j \frac{\partial \gamma_j}{\partial \bar{z}}$$

Now if f is close to conformal, then all the S_j can be approximated as a constant value independent of j, thus

$$\frac{\partial f}{\partial z} \approx \sum_{i=1}^{n}\frac{\hat{e}_j}{e_j}\gamma_j, \qquad \frac{\partial f}{\partial \bar{z}} \approx 0 \qquad (18)$$

which is easily computed and can be used to update z_n in (17).

The gradient approximation (18) for f close to conformal is justified especially in our scenario of a discrete conformal map of a polygonal mesh, since each individual polygon will be close to be conformally mapped (see e.g. the individual polygons in Fig. 6). Since the Newton-Raphson method is relatively tolerant to error in the gradient as long as it points in approximately the right direction, it corrects itself at the expense of more iterations.

In our implementation we initialized z_0 to be the *reverse mapping* of w, i.e. the point that w is mapped to using the barycentric mapping obtained when the roles of the source and target polygons are reversed. This, in itself, is an excellent approximation for the inverse when the mapping is "well-behaved", certainly if it is close to conformal. Experimental results show that this iteration converges rapidly (within a small number of iterations) for regular source polygons. Fig. 10 shows the inverted mean value (MV) map of a regular hexagon to another hexagon computed using this method. The inversion procedure required 7 iterations on the average to converge for each of the vertices of the triangulation of the interior of the target polygon that it was applied to, and no more than 14 iterations in the worst case. The iterative algorithm was implemented as a shader in GLSL (OpenGL Shader Language) to facilitate texture mapping.

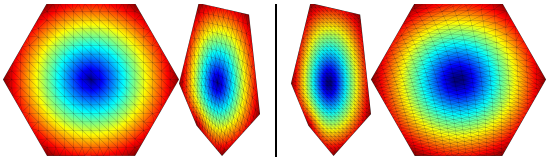

Figure 10: ***(left)*** *A mean value (MV) mapping (left) of a regular hexagon and* ***(right)*** *its inverse computed using the iterative algorithm of Section 6.2. Both mappings are computed on the vertices of a triangulation of the interior of the (source or target) hexagon. On the average, 7 iterations per vertex were required to invert the mapping.*

We note that the recent paper of Chen and Gotsman [CG16b] presented a similar algorithm to invert barycentric mappings. However, in that paper they deal with the transfinite case (i.e. the case of mapping of the interior of a smooth contour) without explicit dicretization. They develop (more complicated) explicit expressions for the gradients of the mapping without making the simplifying assumption that all the S_j can be approximated as a constant, which is justified only in the case of a mesh of multiple elements undergoing a close to conformal mapping.

7 Discussion and Conclusion

We have shown how to generalize the classical quadratic conformal energy associated with deformations of triangle meshes to the case where the mesh consists of regular squares or hexagons. This also takes into account the mapping of the interior of the polygon using barycentric coordinates (which could be harmonic or some approximation of that). We have demonstrated that an interior mapping which in essence is equivalent to triangulating the polygon is particularly bad, and other barycentric mappings which are much closer to a harmonic map are to be preferred, in particular the MLS mapping. Using meshes of higher-order regular polygons, e.g. squares or hexagons, result in faster convergence of the discrete approximation to the continuous limit, for the same number of mesh vertices.

We show that although the Laplace coordinates (which are identical to the Wachspress coordinates for regular polygons) indeed are a good approximation to the harmonic case, an even better approximation is obtained using the so-called Moving Least Squares (MLS) coordinates [MS10]. This is consistent with the findings of Chen and Gotsman [CG16a], who prove that the MLS coordinates are pseudo-harmonic, namely coincide with the classical harmonic Poisson kernel [Ahl79] when the number of vertices of the source polygon is increased and it converges to a circle.

Conformal energy matrices are typically sparse. However, it is important to note that the entries of C corresponding to diagonals of the polygon P will typically vanish only under very special conditions. A similar observation was made by Alexa and Wardetsky [AW11] in their study of Laplacian operators for polygonal meshes.

The general case of a higher-order polygon may be reduced to the triangle case by consistently triangulating both the source and target polygons and mapping each source triangle independently to its target counterpart. This results in a piecewise-affine C^0 mapping and may also be expressed using barycentric coordinate functions (which we labeled T in

the text). In this case, the j'th barycentric function is supported only on the triangles incident on the j'th vertex. Furthermore, the conformal energy matrix C is just the sum of the conformal energy sub-matrices corresponding to the individual triangles, so that the interior edges have entry $\frac{1}{4}\left(\cot\alpha_{jk}+\cot\beta_{jk}\right)$, where α_{jk} and β_{jk} are the two angles opposite the edge. Boundary edges have entry $\frac{1}{4}(i+\cot\alpha_{jk})$, where α_{jk} is the single angle opposite the edge. The results of Chen et al [CXGL10] imply that, among all possible triangulations, the conformal energy is minimized by the Delaunay triangulation of the polygon.

The meshes we use consist of identical regular polygons. It should be possible to generalize to meshes of irregular polygons, possibly conforming to some underlying image content. Irregular meshes of convex elements were used for elasticity computations in the 3D scenario treated by Wicke et al [WBG08]. Similarly, Huang et al [HCLB09] used meshes of irregular tetrahedra for 3D deformation. The latter, however, considered As-Rigid-As-Possible (ARAP) deformations with regularlization for smoothness control, as opposed to our pure conformal deformations. While the use of an irregular mesh will require the computation of a different stiffness matrix for each individual element, the computation is done only once in a pre-processing step when the mesh is constructed. In constrast, the solution of (15) is performed repeatedly as the point constraints are moved in an interative editing session. Using such irregular meshes could be a topic for future work.

Weighting the conformal energy of the individual polygons is useful in practical applications (especially in content-aware image deformation) where distortion is less tolerated in specific regions. In this case a single positive real weight is associated with each polygon. A similar concept has been proposed for so-called "weighted triangulations" [DMMD14], where a real weight is associated with each *vertex* of a triangulation, inducing a generalized (cotangent) Laplacian. We speculate that this is somewhat analogous to our weighting notion, albeit on the *dual* mesh – where each face is dualized to a vertex.

While we have dealt only with approximation of point-to-point conformal maps of compact domains using discrete finite elements, it is also possible to employ the so-called Boundary Element Method (BEM) [WG10]. Here the map is approximated by a linear combination of a finite number of conformal basis functions centered at select locations (which may also be the locations of the constraints), and the coefficients are computed such that the user-provided constraints are satisfied. This is similar in spirit to the classical Radial Basis Function (RBF) method and resembles the MLS method mentioned in Section 5.2. However, while the resulting map will be conformal (as opposed to approximately conformal in our method), the results are extremely sensitive to the character of the basis functions used and the number of degrees of freedom, thus somewhat unpredictable away from the constraints.

Our formulation of the conformal mapping problem involved the convenient use of complex numbers. While this is extremely convenient in the plane, there is no direct analog in higher dimensions, in particular three dimensions. Fortunately, some of the properties of complex numbers can be extended into 3D using vector analysis.

Acknowledgment

R. Chen has been supported by the Max Planck Center for Visual Computing and Communication.

References

[Ahl79] L. Ahlfors. *Complex Analysis* (3rd Ed.), McGraw-Hill, 1979.

[AW11] M. Alexa and M. Wardetzky. Discrete Laplacians on general polygonal meshes. *ACM Transactions on Graphics (Proc. ACM SIGGRAPH),* 30(4):102:1--102:10, 2011.

[BF15] A. Belyaev and P. Fayolle. On transfinite Gordon-Wixom interpolation schemes and their extensions. *Computers & Graphics,* 2015.

[CMMS13] C. Cartade, C. Mercat, R. Malgouyres and C. Samir. Mesh parameterization with generalized discrete conformal maps. *J. Math. Imaging Vis*., 46:1–11, 2013.

[CXGL10] R. Chen, Y. Xu, C. Gotsman and L. Liu. A spectral characterization of the Delaunay triangulation. *Computer Aided Geometric Design*, 27(4):295-300, 2010.

[CG16] R. Chen and C. Gotsman. Generalized as-similar-as-possible warping with applications in digital photography. *Computer Graphics Forum* (*Proc. Eurographics*), 35(2):81-92, 2016.

[CG16a] R. Chen and C. Gotsman. On pseudo-harmonic barycentric coordinates. *Computer-Aided Geometric Design,* 44:15-35, 2016.

[CG16b] R. Chen and C. Gotsman. Complex transfinite barycentric mappings with similarity kernels. *Computer Graphics Forum (Proc. Symp. Geom. Proc.)*, 35(5):41-53, 2016.

[DMMD14] F. de Goes, P. Memari, P. Mullen, and M. Desbrun. Weighted triangulations for geometry processing. *ACM Transactions on Graphics (Proc. SIGGRAPH)*, 33(3), 2014.

[DMA02] M. Desbrun, M. Meyer, and P. Alliez. Intrinsic parameterizations of surface meshes. *Computer Graphics Forum (Proc. Eurographics)*, 21(3):209-218, 2002.

[Dur04] P. Duren. *Harmonic Maps in the Plane.* Cambridge Tracts in Math. 156. Cambridge University Press, 2004.

[Flo03] M. Floater. Mean-value coordinates. *Computer Aided Geometric Design*, 20(1):19-27, 2003.

[Flo15] M. Floater. Generalized barycentric coordinates and applications. *Acta Numerica*, 24:161-214, 2015.

[FHK06] M. Floater, K. Hormann, G. Kós. A general construction of barycentric coordinates over convex polygons. *Advances in Computational Mathematics*, 24:311-331, 2006.

[GW74] W.J. Gordon, J.A. Wixom. Pseudo-harmonic interpolation on convex domains. *SIAM Journal on Numerical Analysis*, 11:909-933, 1974.

[HKA15] P. Herholtz, J.-E. Kyprianidis and M. Alexa. Perfect Laplacians for polygon meshes. *Computer Graphics Forum (Proc. Symp. Geometry Proc.),* 34(5), 2015.

[HF06] K. Hormann, M.S. Floater. Mean value coordinates for arbitrary planar polygons. *ACM Transactions on Graphics*, 25:1424-1441, 2006.

[HJ13] R.A. Horn and C.R. Johnson. *Matrix Analysis (2nd Ed.)*. Cambridge University Press, 2013.

[HCLB09] J. Huang, L. Chen, X. Liu and H. Bao. Efficient mesh deformation using tetrahedron control mesh, *Computer Aided Geometric Design*, 26:617-626, 2009.

[JMD*07] P. Joshi, M. Meyer, T. DeRose, B. Green and T. Sanocki. Harmonic coordinates for character articulation. *Proc. ACM SIGGRAPH*, 2007.

[LM02] B. Levy and J. Maillot. Least squares conformal maps for automatic texture atlas generation. *Proc. ACM SIGGRAPH*, 21(3):362-371, 2002.

[MS10] J. Manson and S. Schaefer. Moving least squares coordinates. *Computer Graphics Forum (Proc. Symp. Geom. Proc.)*, 29(5):1517-1524, 2010.

[MRS14] G. Manzini, A. Russo and N. Sukumar, New perspectives on polygonal and polyhedral finite element methods. *Math. Models Methods Appl. Sci.* 24:1665, 2014.

[MTAD08] P. Mullen, Y. Tong, P. Alliez and M. Desbrun. Spectral conformal parameterization. *Computer Graphics Forum* (*Proc. Symp. Geom. Proc.*), 27(5):1487-1494, 2008.

[PP93] U. Pinkall and K. Polthier. Computing discrete minimal surfaces and their conjugates. *Experiment. Math.*, 2(1):15-36, 1993.

[PL14] R. Poranne, Y. Lipman**.** Provably good planar mappings. *ACM Transactions on Graphics (Proc. SIGGRAPH),* 33(4), 2014.

[RGSS10] M. Rubinstein, D. Gutierrez, O. Sorkine and A. Shamir. A comparative study of image retargeting. *ACM Transactions on Graphics (Proc. SIGGRAPH Asia),* 29(6), 2010.

[SMW06] S. Schaefer, T. McPhail and J. Warren. Image deformation using moving least squares. *Proc. ACM SIGGRAPH*, 533-540, 2006.

[SKPS13] C. Schüller, L. Kavan, D. Panozzo, and O. Sorkine-Hornung. Locally injective mappings. *Computer Graphics Forum* (*Proc. Symp. Geom. Proc.*), 125-135, 2013.

[SM06] N. Sukumar and E. A. Malsch. Recent advances in the construction of polygonal finite element interpolants, *Arch. Comp. Meth. Engng*, 13(1):129–163, 2006.

[Wac75] E.L. Wachspress. A rational finite element basis, in: *Mathematics in Science and Engineering*, vol. 114, Academic Press, 1975.

[WBGH11] O. Weber, M. Ben-Chen, C. Gotsman and K. Hormann. A complex view of barycentric mappings. *Computer Graphics Forum (Proc. Symp. Geom. Proc.*), 30(5):1533-1542, 2011.

[WG10] O. Weber and C. Gotsman. Controllable conformal maps for shape deformation and interpolation. *ACM Transactions on Graphics (Proc. SIGGRAPH)*, 29(4), 2010.

[WBG08] M. Wicke, M. Botsch and M. Gross. A finite element method on convex polyhedra. *Computer Graphics Forum (Proc. SGP)*, 26(3):355-364, 2007.